Nanoscale

Accepted Manuscript

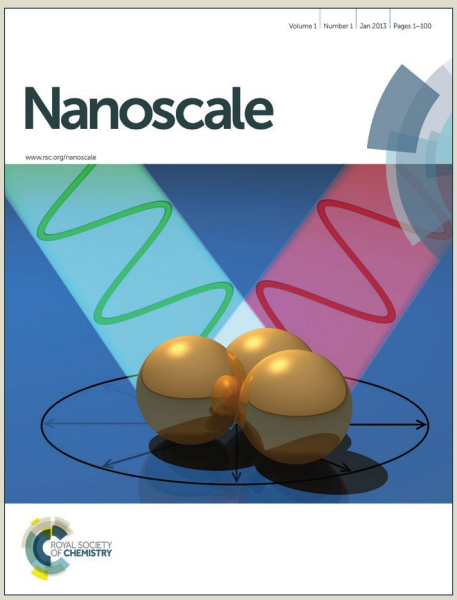

ROYAL SOCIETY OF CHEMISTRY

www.rsc.org/nanoscale

Nanoscale

ARTICLE

Ultra-Stable Small Diameter Hybrid Transition Metal Dichalcogenide Nanotubes *X*-M-*Y* (X, Y = S, Se, Te; M = Mo, W, Nb, Ta): A Computational Study

Received 00th January 20xx,
Accepted 00th January 20xx

DOI: 10.1039/x0xx00000x

www.rsc.org/

Wen Zhao,[a,b] Yuanchang Li,[c] Wenhui Duan [b] and Feng Ding [a]

Similar to graphene and hexagonal boron nitride (h-BN), the two-dimensional (2D) transition metal dichalcogenide (TMD) can be rolled into one-dimensional (1D) nanotubes. While, owing to their three-atom-thick structure, the large energy penalty greatly hinders the synthesis of small diameter TD nanotubes. Here we propose the synthesis of hybrid TMD nanotubes with different chalcogen on each side (*X*-TM-*Y*) by self-assembly rolling up. Our calculations indicate the tube formation can be driven by the relaxation of the intrinsic strain in *X*-TM-*Y* and the hybrid nanotubes as small as ~ 2.0 nm could be synthesized. The rich variety of polymorphs exhibit unique and tunable electronic properties. Our finding opens a door to synthesize hybrid small diameter TMD nanotubes for various applications.

1. Introduction

The first report on synthesis of WS_2 nanotubes (NTs) in 1992[1] triggered extensive research on transition metal dichalcogenides (TMDs) tubular structures. They were proved to have outstanding physical and mechanical properties for a plethora of applications, such as field-effect transistors[2], nanoscale optoelectronic devices[3], solid lubricants[4], self-lubricating coatings for medical usage[5], additives in high-strength and high-toughness nanocomposites[6, 7], and a variety of other potential applications.

It is known that the properties of TMD NTs are diameter dependent, due to the quantum confinement effects of electrons. For example, small TMD NTs have tunable band gaps[8] and were proved to have larger breaking strain[9]. Besides, the hollow space inside the tube wall can be used as templates for synthesizing various one dimensional (1D) nanomaterials, a confined space for chemical reactions, storage of various gases etc. Thus, synthesizing small-diameter TMD NTs is greatly desired.

However, different from the one-atom-thick graphene or hexagonal boron nitride (h-BN), the three-atoms-thick TMDs are hard to be bent or rolled and therefore synthesizing small NTs is extremely difficult. Intuitively, during the formation of tubular structure from a flat sheet, an internal strain is built. The curvature energy penalty is proportional to the bending stiffness[10]

$$\frac{\mathrm{Y}h^3}{12(1-\nu^2)}k^2 \sim \frac{h^3}{R^2} \qquad (1)$$

where $k = 1/R$ is the curvature of the tube wall, Y is Young's modulus, h is the effective thickness, v is the Poisson's ratio, and R is the radius of the tube. Because the effective thickness for bending a typical TMD layer ($h \sim 0.3$ nm[11]) is much larger than that of graphene ($h \sim 0.077$ nm[12]), only large TMD tubes can be stable. It has been reported theoretically [13, 14] and experimentally [14] that a TMD nanotube is more stable than a TMD strip only when its diameter is larger than 6 nm (see **Figure 1(e)**), while the critical diameter for carbon NT is only 2 nm. This simple theoretical estimation is in good agreement with experimental observations, where most synthesized TMD NTs have diameters larger than 10 nm [15] while carbon NTs with diameter ~ 1 nm have been synthesized.

[a] Institute of Textiles and Clothing, Hong Kong Polytechnic University, Hong Kong, China.
[b] State Key Laboratory of Low-Dimensional Quantum Physics and Collaborative Innovation Center of Quantum Matter, Department of Physics, Tsinghua University, Beijing 100084, China.
[c] National Center for Nanoscience and Technology, Beijing 100190, China.
† Electronic Supplementary Information (ESI) available: See
DOI: 10.1039/x0xx00000x

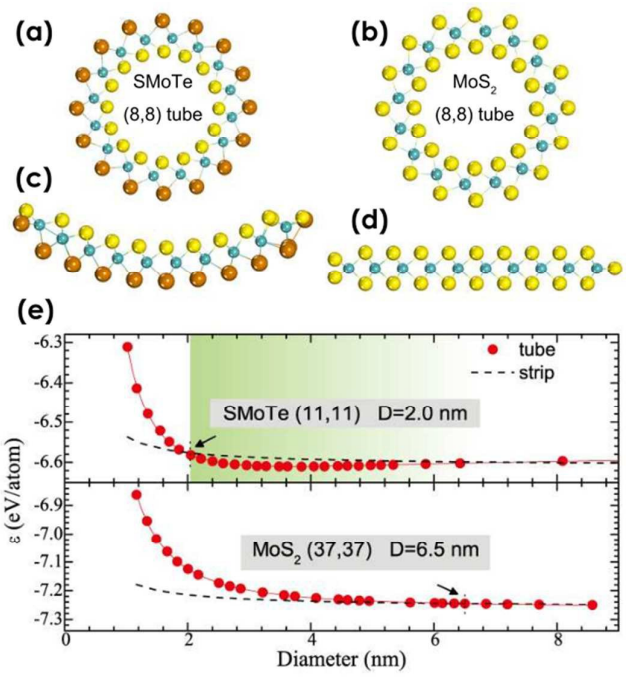

Fig. 1 Relaxed atomic structures of (a) SMoTe and (b) MoS_2 tubes and (c) SMoTe and (d) MoS_2 strips in a unit cell. The strips are reconstructed with 50% chalcogen on both edges[16, 17]. (e) Energy per atom of SMoTe and MoS_2 tubes and strips (with the same number of atoms), as a function of tube diameter (*D*). The arrows label the critical diameter of strip-tube transitions. The green borderline denotes the lower diameter limit of SMoTe tubes.

Here, in order to reduce the curvature energy penalty, we propose to synthesize the hybrid TMD NTs by breaking the symmetry of TMD along the thickness direction. By placing large chalcogen atoms (e.g., Te) on one side of the TMD and smaller chalcogen atoms (e.g., S) on the opposite side, a natural build-in strain is developed in the 2D TMD, where the large chalcogen atoms are compressed and the small chalcogen atoms are stretched. By spontaneously rolling the flat hybrid TMD sheet into a tube with the small chalcogen atoms inside (**Figure 1(a)**), the strains on both sides can be released notably. We denote this class of asymmetrical hybrid TMDs or NTs as *X*-TM-*Y*, whose atomic coordinates are nearly as same as the original TMX_2 NTs[8] only with different element species and lattice constants (The structure files are available in the Supplemental Material). Because of the greatly reduced curvature energy penalty, synthesizing hybrid TMD NTs might be easily achieved.

2. Model and calculations

In this study, a geometrical model is developed to explore the stability of twelve *X*-TM-*Y* hybrid NTs (*X*, *Y* = S, Se, Te; TM = Mo, W, Nb, Ta) and density functional theory (DFT) calculations are performed to verify the model, using the Vienna Ab initio Simulation Package (VASP)[18]. The exchange-correlation potential is described by the PBE version of GGA[19] and the core region by the projector augmented wave method[20]. High accuracy settings are adopted in all calculations. For one-dimensional periodic cells that contain up to 300 atoms, a dense k-point mesh (1×1×11) is used for Brillouin zone sampling. The plane-wave cutoff is set to 280 eV, and a conjugate gradient method is applied to relax the geometry until interatomic forces are less than 0.01 eV/Å. For rigorous testing the stability of fully relaxed hybrid NTs, we calculate phonon frequencies using the finite-displacement approach as implemented in the Phonopy code[21] with higher accuracy settings[22].

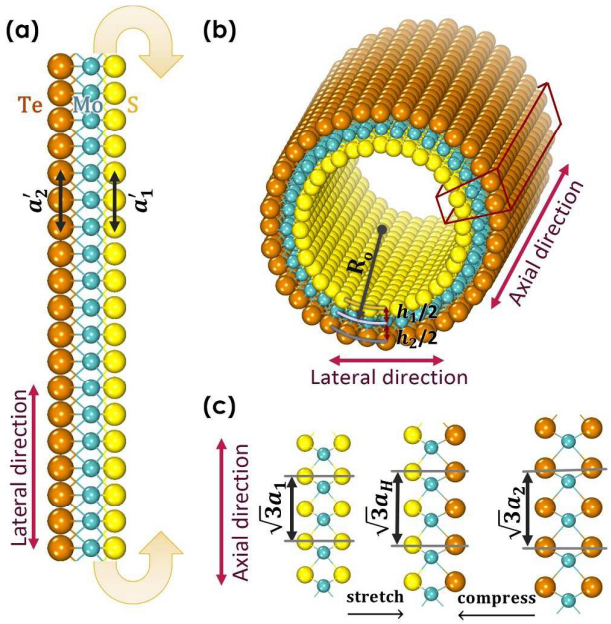

Fig. 2 The schematic view of the hybrid TMD NT, taking zigzag (12, 0) SMoTe tube as an example. When a flat SMoTe monolayer (a) is rolled into a SMoTe NT (b), the axial lattice constant of the tube becomes different from that of either MoS_2 or $MoTe_2$ tube with the same size (c). It will affect the lateral lattice constant (a) due to Poisson's effect. The grey lines in (c) are the periodic boundaries in calculations.

3. Results and analysis

In order to have an intuitive understanding on the stability of a hybrid tube vs. the corresponding hybrid strip (or an unfolded tube with two edges), we compare the energies of SMoTe/MoS_2 NTs and strips, as plotted in **Figure 1(e)**. For a strip, we suppose the total number of atoms N in a unit cell of calculation consists of N_x atoms at the boundaries and N_i atoms inside the strip[14] ($N = N_i + N_x$), and the corresponding energy/atom is denoted as ε_x and ε_∞. So the energy of a strip can be calculated as

$$E_s = N_i\varepsilon_\infty + N_x\varepsilon_x \quad (2)$$

In our case $N_x = 3$ and then $N_i = N - 3$ (See the structure files in the Supplemental Material.). Therefore, the energy per atom for a strip can be written as

$$\varepsilon = \frac{E_s}{N} = \varepsilon_\infty + \frac{3}{N}(\varepsilon_x - \varepsilon_\infty) \quad (3)$$

Using two strips with different width (different N), combined with E_s from DFT calculations, we can obtain parameters ε_x (-6.309 eV for MoS_2 and -5.894 eV for SMoTe) and ε_∞ (-7.258 eV for MoS_2 and -6.609 eV for SMoTe), and plot the whole range of ε for strips as shown in **Figure 1(e)**.

The critical diameter of SMoTe, D_{s-t} in **Figure 1(e)**, is found to be only 2.0 nm, while that of MoS_2 is as large as 6.5 nm, which is in agreement with previous calculations[14]. These results clearly indicate the exceptional stability of hybrid TMD NTs in relative to hybrid TMD layers. As will be seen later, the great D_{s-t} difference stems from the self-folding tendency of the asymmetric *X*-TM-*Y* structure. This result sets up a lower diameter limit of growing hybrid *X*-TM-*Y* NTs under the near thermal equilibrium condition.

Now, let's elaborate how to use our classical model to obtain the optimal radius of the self-folded hybrid NTs. We use a zigzag (ZZ) SMoTe hybrid NT as an example (see **Figure 2**), in which the parameters are derived from the *monolayer* in-plane lattice constants[23]. Here we denote (a_1, h_1) as the homoelemental distance of MoS_2 (i.e. Mo-Mo distance) and its thickness, and (a_2, h_2) for $MoTe_2$. Suppose the relaxed structure of SMoTe NT has equal S-S/Te-Te distance as that in MoS_2/$MoTe_2$ monolayer, its optimal radius R_O can be calculated by solving the equation

$$\frac{a_1}{R_0 - \frac{h_1}{2}} = \frac{a_2}{R_0 + \frac{h_2}{2}} \quad (4)$$

However, to be more rational, we have taken into account the Poisson's effect. Intuitively, the homoelemental distance and thickness of a hybrid SMoTe can be estimated as (a_H, h_H), where $a_H = (a_1+a_2)/2$ and $h_H = (h_1+h_2)/2$. When a flat SMoTe monolayer is rolled into a ZZ tube, we suppose its axial direction (also armchair direction, AC) lattice constant is fastened with $\sqrt{3}a_H$ (see **Figure 2(c)** and **Figure SI** in the supplemental material), which indicates the S-S distance along the axial direction is stretched by (a_H - a_1)/a_1 compared to that in pure MoS_2 tube, while the Te-Te distance is compressed by (a_2 - a_H)/a_2. It will accordingly affect the S-S and Te-Te distance in the lateral direction due to Poisson's effect. The relationship between the new homoelemental distances (a'_1, a'_2) and (a_1, a_2) can be written in a compact form:

$$\frac{a_i' - a_i}{a_i} = -\nu_i \frac{a_H - a_i}{a_i}, (i = 1, 2) \quad (5)$$

where ν_1 and ν_2 are the Poisson's ratios of MoS_2 and $MoTe_2$, respectively [24]. Then the optimal radius, R_O, can be calculated as

$$R_O = \frac{a'_1 h_2 + a'_2 h_1}{2(a'_2 - a'_1)} \quad (6)$$

From above results, we can clearly see that the optimal diameter sensitively depends on the atomic size difference between the chalcogenide on both sides of the NT. Larger atomic size difference leads to smaller optimal hybrid NTs.

Besides, the optimal radius, R_{DFT}, of the NT can be obtained from DFT calculations by calculating the energy of the hybrid NTs:

$$\varepsilon_c = \alpha(k - k_0)^2 + \varepsilon_{c0} \quad (7)$$

where ε_c is the energy difference per atom between a NT and a corresponding flat TMD monolayer, which is proportional to k^2, where $k \sim 1/R$ is the curvature of the tube, $k_0 \sim 1/R_{DFT}$ is the curvature of the optimized NT. ε_{c0} is the energy difference between the optimal NT and a flat TMD layer. α is a constant which depends on the Young's modulus, effective thickness and volume of the material [25].

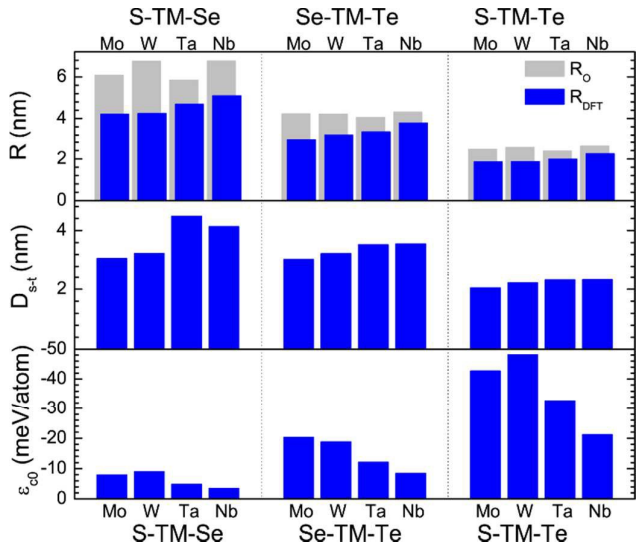

Fig. 3 The optimal radii obtained from the model (R_O) and from DFT calculations (R_{DFT}), the strip-tube transition diameter (D_{s-t}), and the energy difference between a hybrid tube and the corresponding monolayer (ε_{c0}), for each *X*-TM-*Y* NT.

The results from above geometrical model and DFT fitting of eq. (7) for the twelve *X*-TM-*Y* hybrid NTs are shown in **Figure 3** and **Table SI** of the Supplemental Material. We can see that, R_{DFT} is only 10-30% smaller than R_O, which proves the validity of the simple geometrical model. As expected, the optimal radius of the tube highly depends on the differences between a_1 and a_2. Therefore the combination of S-TM-Te leads to the smallest NTs with $R \sim 2.0$ nm. For other hybrid tubes, the optimal radii follow the trend *R*(SMTe) < *R*(SeMTe) < *R*(SMSe), which is insensitive to the selection of transition metal (Mo, W, Nb, or Ta).

Figure 4(a) shows the formation energies of the armchair and zigzag structured MoS_2, $MoTe_2$, and SMoTe tubes, as a function of tube wall curvature. Here, negative curvatures correspond to an inside-out tube, e.g. the SMoTe tube with Te outside turns into TeMoS tube with S outside. The formation energy ε_f of a SMoTe NT is defined as

$$\varepsilon_f = \frac{E_t(\mathrm{SMoTe}) - \frac{1}{2}[E_{ml}(\mathrm{MoS_2}) + E_{ml}(\mathrm{MoTe_2})]}{N} \qquad (8)$$

where $E_t(\mathrm{SMoTe})$, $E_{ml}(\mathrm{MoS_2})$ and $E_{ml}(\mathrm{MoTe_2})$ are the calculated energies of the SMoTe tube, MoS_2 and $MoTe_2$ flat layers with the same number of atoms *N*, respectively, and *N* is the number of atoms in a unit cell of calculation. As seen from **Figure 4(a)**, ε_f (data points) of all ZZ and AC NTs can be well fitted by $\varepsilon_f \sim \alpha(k\text{-}k_0)^2$ (lines in **Figure 4(a)**) and the coefficient α slightly depends on the chirality of the tube, where AC tubes are more stable than ZZ ones. For traditional TMX_2 NTs, $\varepsilon_f = [E_t(\mathrm{MoX_2}) - E_{ml}(\mathrm{MoX_2})]/N$, we can see that $k_0 = 0$, i.e., the flat MoX_2 is most stable . While for hybrid NTs, their natural inclination of rolling up leads to a tubular ground energy structure ($k_0 \neq 0$). For SMoTe, $k_0 = 0.52$ nm^{-1}, or $R_0 = 1.9$ nm ($D_0 = 3.8$ nm). Such a diameter corresponds to the AC (21, 21) tube or the ZZ (36, 0) tube, whose structure files are available in the Supplemental Material.

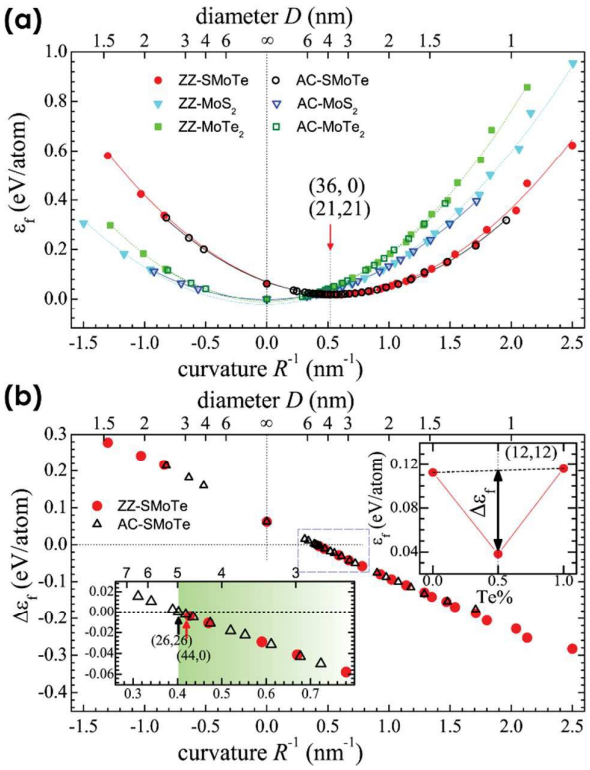

Fig. 4 (a) The formation energies of armchair (AC) and zigzag (ZZ) SMoTe, MoS_2 and $MoTe_2$ NTs. Lines are best fitting parabola. (b) $\Delta\varepsilon_f$ vs. curvature in all-diameter range of AC and ZZ SMoTe tubes, where the part in the rectangle is enlarged in the lower inset and the green borderline in it denotes the upper diameter limit of SMoTe tubes. The upper inset shows formation energies (red dots) of a (12, 12) NT of different Te concentration: 0% (MoS_2), 50% (SMoTe), and 100% ($MoTe_2$). At Te=50%, the energy difference of the red dot and the black dash line is $\Delta\varepsilon_f$.

Figure 4(b) shows the formation energy difference between a hybrid tube and two traditional NTs with the same number of Mo atoms, which is defined by

$$\Delta\varepsilon_f = \varepsilon_f(\mathrm{SMoTe}) - \frac{1}{2}\left[\varepsilon_f(\mathrm{MoS_2}) + \varepsilon_f(\mathrm{MoTe_2})\right] \quad (9)$$

It can be clearly seen that $\Delta\varepsilon_f$ becomes negative at the critical diameter of D_C = 4.8 nm (or R_C = 2.4 nm), which corresponds to the (26, 26) AC tube or the (44, 0) ZZ tube. Negative formation energy implies that growing a hybrid NT (SMoTe) is energetically more favourable than growing a MoS_2 tube and a $MoTe_2$ tube. Taking the (12, 12) tube as an example, as shown in the inset of **Figure 4(b)**, if we have the same amount of Mo, S and Te powder sources, the energy cost to grow two separated tubes (MoS_2 with Te% = 0 and $MoTe_2$ with Te% = 1) is 76 meV/atom higher than that to grow a hybrid tube (SMoTe with Te% = 0.5). This result sets up an upper limit of the diameter of the hybrid NTs synthesized under the near thermal equilibrium condition.

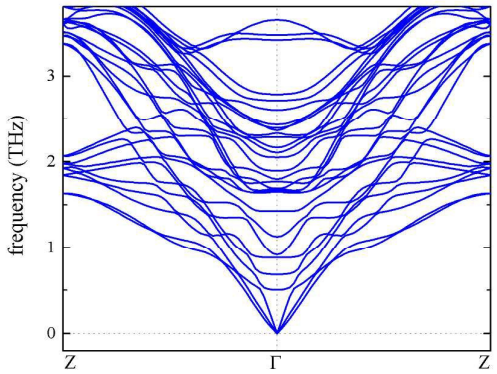

Fig. 5 The phonon–dispersion curves of SMoTe armchair (5, 5) nanotube.

The results above guarantee the relative stability of a hybrid NT versus a strip or other NT constitutions. To ensure the intrinsic stability of the hybrid NT, the phonon calculations for SMTe (5, 5) NT are performed. As shown in Figure 5, no imaginary phonon frequencies exist throughout the Brillouin zone, suggesting the hybrid NT is dynamically stable.

Finally let us consider the electronic properties of the SMoTe NTs as an example. **Figures 6(a)** and **6(b)** show the band gap as a function of tube curvature and **Figure 6(c)** shows band structures of the AC and ZZ NTs with the optimal radius. As expected, AC NTs have indirect gaps while ZZ NTs have direct gaps, akin to the TMDs NTs [8]. However, for MoS_2 NTs, the band gap increases monotonously when diameter increase [8]. Whereas for the band gap of both ZZ and AC SMoTe NTs, a peak appears at k ~ 0.65 nm^{-1}. The emergences of maximum band gap can be attributed to the fully released strain and the high stability of the optimal tube.

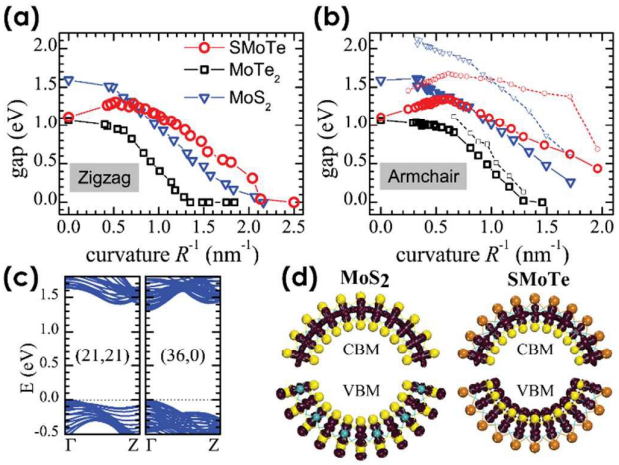

Fig. 6 Band gaps vs. curvature of zigzag (a) and armchair (b) SMoTe, MoS_2 and $MoTe_2$ NTs. In (b) the smaller points correspond to the direct gaps of the indirect-gap semiconductors. (c) Band structures of (21, 21) and (36, 0) SMoTe NTs. Zero is the valence band maximum. (d) Real-space charge distribution (maroon) at Γ point of (12, 0) MoS_2 and SMoTe tubes with an isosurface = 0.006 e/Å^3. The distribution for $MoTe_2$ tube is similar to that for MoS_2 tube, so not present here.

The analysis from the local density of states reveals that the conduction band minimum (CBM) is mainly contributed by $d_{x^2-y^2}$ orbitals of Mo, the same as that in MoS_2 or $MoTe_2$ NTs, while the valence band maximum (VBM) is mainly attributed by the coupling between d_{z^2} orbitals of Mo and the p orbitals of innermost S. Unlike the contribution to the VBM from the outermost S atoms in MoS_2 NTs or the outermost Te atoms in $MoTe_2$ NTs, the electronic states of the outermost Te atoms in SMoTe NTs are far from the Fermi level, indicating a less active outside surface of SMoTe NTs. These characters are representatively illustrated in **Figure 6(d)** by comparing the real-space charge distribution at the VBM and CBM of (12,0) MoS_2 and SMoTe NTs. The bending curvature induced active inside wall and inert outside wall renders the tube a perfect confinement for the self-assembly growth of 1D nanowire and immune to the possible pollution outside the tube.

4. Conclusions

In summary, through systematic analysis and DFT calculations, the high stability of hybrid TMDs NTs, *X*-TM-*Y*, is confirmed. For the well-studied example, SMoTe, the optimal diameter ranges from 2.0 to 4.8 nm, where the NT structure is more stable than the corresponding strip or the traditional TMX_2 tubes. Our study also reveals that the hybrid *X*-TM-*Y* tubes have unique electronic properties. For example, the SMoTe has a maximum gap ~1.3 eV at *D* ~ 3.1 nm, an active inner surface, and an inert outer surface. This study opens a way of synthesizing and using the small diameter transition metal dichalcogenides for various applications.

Acknowledgements

We acknowledge the fruitful discussions with Dr. Jianing Zhuang, Dr. Pengcheng Chen, Dr. Jia Li and Dr. Luchi Yao. The support of NSFC research grants (#21273189) and Hong Kong RGC-GRF grants (BQ-26K, B-Q35N, B-Q41N) are acknowledged. WZ and WD also thank the Ministry of Science and Technology of China (Grant Nos. 2011CB606405 and 2011CB921901) and National Natural Science Foundation of China (Grant No. 11334006). Our computation is completed on the Explorer 100 cluster system of Tsinghua National Laboratory for Information Science and Technology. The acknowledgements come at the end of an article after the conclusions and before the notes and references.

Notes and references

1. R. Tenne, L. Margulis, M. e. a. Genut and G. Hodes, *Nature*, 1992, **360**, 444-446.
2. R. Levi, O. Bitton, G. Leitus, R. Tenne and E. Joselevich, *Nano Lett.*, 2013, **13**, 3736-3741.
3. C. Zhang, S. Wang, L. Yang, Y. Liu, T. Xu, Z. Ning, A. Zak, Z. Zhang, R. Tenne and Q. Chen, *Appl. Phys. Lett.*, 2012, **100**, 243101.
4. L. Rapoport, Y. Bilik, Y. Feldman, M. Homyonfer, S. Cohen and R. Tenne, *Nature*, 1997, **387**, 791-793.
5. A. Katz, M. Redlich, L. Rapoport, H. Wagner and R. Tenne, *Tribol. Lett.*, 2006, **21**, 135-139.
6. M. Naffakh, C. Marco, M. A. Gómez and I. Jiménez, *J. Phys. Chem. B*, 2008, **112**, 14819-14828.
7. X. Zou, Y. Liu and B. I. Yakobson, *Nano Lett.*, 2013, **13**, 253-258.
8. G. Seifert, H. Terrones, M. Terrones, G. Jungnickel and T. Frauenheim, *Phys. Rev. Lett.*, 2000, **85**, 146.
9. K. Nagapriya, O. Goldbart, I. Kaplan-Ashiri, G. Seifert, R. Tenne and E. Joselevich, *Phys. Rev. Lett.*, 2008, **101**.
10. G. G. Tibbetts, *J. Cryst. Growth*, 1984, **66**, 632-638.
11. X. Wu, Z. Xu and X. Zeng, *Nano Lett.*, 2007, **7**, 2987-2992.
12. B. I. Yakobson, C. Brabec and J. Bernholc, *Phys. Rev. Lett.*, 1996, **76**, 2511.
13. T. Lorenz, D. Teich, J.-O. Joswig and G. Seifert, *J. Phys. Chem. C*, 2012, **116**, 11714-11721.
14. G. Seifert, T. Köhler and R. Tenne, *J. Phys. Chem. B*, 2002, **106**, 2497-2501.
15. R. Tenne and M. Redlich, *Chem. Soc. Rev.*, 2010, **39**, 1423-1434.
16. S. Helveg, J. V. Lauritsen, E. Lægsgaard, I. Stensgaard, J. K. Nørskov, B. Clausen, H. Topsøe and F. Besenbacher, *Phys. Rev. Lett.*, 2000, **84**, 951.
17. J. V. Lauritsen, J. Kibsgaard, S. Helveg, H. Topsøe, B. S. Clausen, E. Lægsgaard and F. Besenbacher, *Nat. Nanotechnol.*, 2007, **2**, 53-58.
18. G. Kresse and J. Furthmüller, *Comput. Mater. Sci.*, 1996, **6**, 15-50.
19. J. P. Perdew, K. Burke and M. Ernzerhof, *Phys. Rev. Lett.*, 1996, **77**, 3865.
20. P. E. Blöchl, *Phys. Rev. B*, 1994, **50**, 17953.
21. A. Togo, F. Oba and I. Tanaka, *Phys. Rev. B*, 2008, **78**, 134106.
22. Here phonon calculations are performed in the SMoTe armchair (5, 5) nanotube, using 1×1×8 large supercells consisting of 240 atoms to fully consider the lattice interactions. Since calculating the real-space force constants of the supercell needs accurate total energy, we improve the plane-wave cutoff to 400 eV. 100 iterations of symmetrization are applied to symmetrize the force constants partly in the Phonopy package.
23. Y. Ding, Y. Wang, J. Ni, L. Shi, S. Shi and W. Tang, *Physica B*, 2011, **406**, 2254-2260.
24. J. Kang and J. Li, in MoS_2, Springer, 2014, pp. 77-101.
25. O. Gülseren, T. Yildirim and S. Ciraci, *Phys. Rev. B*, 2002, **65**.